Inverted Hysteresis, Magnetic Domains and Hysterons

Ivan Soldatov[1], Petru Andrei[3], and Rudolf Schäfer[1,2]
[1]Leibniz Institute for Solid State and Materials Research (IFW) Dresden, Helmholtzstrasse 20, D-01069 Dresden, Germany
[2]Institute for Materials Science, TU Dresden, 01062 Dresden, Germany
[3]Department of Electrical and Computer Engineering, Florida State University, Tallahassee, Florida 32310, USA

We use MOKE (Magneto-Optical Kerr Effect) magnetometry on extended samples to measure local hysteresis curves as a function of an externally applied field in a magnetostriction-free amorphous ribbon and an elliptical NiFe (Permalloy) film element. Although these materials are magnetically soft and have almost zero coercive field, we found that the *local* hysteresis curves have a highly nonlinear hysteretic character, displaying both counterclockwise and clockwise rotation senses when cycling the loops. This unexpected result can be explained by looking at the total hysteresis curve of the materials as a superposition of local curves and can be described mathematically using the formalism of the Preisach model. Within the framework of this model, we derive the conditions under which a superposition of clock- and counterclockwise hysteresis loops can lead to a hysteresis-less system, and propose a technique to map the hysterons that define the Preisach distribution to physical regions in the specimens.

***Index Terms*—Magnetism in solids, magnetic domains, hysterons, magnetic hysteresis, inverted hysteresis, MOKE magnetometry, Kerr microsccopy, Preisach model.**

I. Introduction

Ferromagnetic amorphous ribbons are soft magnetic materials that have been developed and optimized for numerous applications over the last decades. The magnetization curves of such ribbons are known to present very small or no hysteresis at all and the total energy loss is often negligible [HR13]. In this letter we show that, nevertheless, amorphous ribbons do display highly unusual, clockwise and counterclockwise hysteresis loops when the magnetization is measured *locally* as a function of an externally applied field. This somewhat surprising phenomenon can also be observed in magnetic films if the magnetization reversal is dominated by domain processes. In the next two sections, we present examples of such phenomena for the cases of a magnetostriction-free amorphous ribbon and an elliptical NiFe (Permalloy) film element. Then, in Sect. IV, we introduce a mathematical description of the magnetization curves in both materials based on the classical Preisach model. More importantly, we derive the conditions under which a superposition of clock- and counterclockwise hysteresis loops can lead to a hysteresis-less system, and propose a technique to map the hysterons that define the Preisach distribution to physical regions in the ribbon and permalloy film.

II. Unexpected hysteresis phenomena in amorphous ribbon

The hysteresis curve of a zero-magnetostrictive, cobalt-based, $50\,\mathrm{mm} \times 4.5\,\mathrm{mm} \times 20\,\mu\mathrm{m}$ amorphous ribbon is shown in Fig. 1a. The curve was measured inductively using a fluxmeter and an air-flux-compensated pickup coil close to the middle of the ribbon as indicated in Fig. 1b. The magnetic field was applied along the ribbon's long axis and the sweeping frequency was 0.05 Hz. The field was generated in a 24 cm long solenoid by creating an opening that allowed us to introduce the lens of a Kerr microscope in the center (see Fig. 1c). The drop in magnetic field caused by the opening was compensated by additional windings around the hole to ensure that the field is homogeneous along the center axis of the solenoid. During the measurements, the magnetic domains were imaged by longitudinal wide-field Kerr microscopy [Sch07], [SS17b] using a 2.5× objective lens, which has a field of view sufficiently wide to capture the whole ribbon width within one frame. The 180° magnetic domains, presented in Fig. 1d, are all magnetized along the vertical axis, which is identical to the longitudinal axis along which the field was applied. This indicates the presence of a longitudinal shape anisotropy. If the magnetization curves were measured on a tape-wound core of the same material, a Z-type (i.e. square) loop would be expected [HR13]. The finite ribbon length in our case and the related demagnetization field, enforce a sheared Z-loop that allows us to observe the domains using Kerr microscopy (note that, in case of an unsheared Z-loop, the fast switching by 180° domain wall motion would prohibit to catch the domains in an image). As expected in the case of a good soft magnet, the coercivity of this material is almost vanishing.

Besides for domain imaging, our wide-field Kerr microscope can also be used as MOKE (Magneto-Optical Kerr Effect) magnetometer by plotting the image intensity of a selectable region of interest as a function of the applied magnetic field [SS17a]. Such MOKE loops, obtained in the same ribbon after the pickup coil was removed, are shown in Fig. 1e-g. It is important to notice that MOKE measurements on a bulk material like an amorphous ribbon are only sensitive to surface domains [MSTS15], [LSB$^+$15] within a magneto-optical information depth of about 20 nm [KSFH15]. Yet, for our ribbon this does not present a problem because no traces of a layered domain pattern [HS98] are visible and the observed 180° domains are expected to expand through the depth of the ribbon. A special behavior of the surface domains compared to those in the volume of the ribbon is thus unlikely. As a confirmation of this assumption, we observe that the MOKE

Manuscript received ???, 2020; revised ???. Corresponding author: R. Schäfer (email: r.schaefer at ifw-dresden.de).

loop obtained on a $4.5 \times 3\,\mathrm{mm}^2$ area that covers the entire width of the ribbon (Fig. 1e) is practically identical to the loop measured inductively (Fig. 1a).

Unexpected MOKE hysteresis curves are found when *local* sample areas are evaluated. Two such loops, measured in the two areas marked with white frames in Fig. 1d, are presented in (f) and (g). In both cases, the coercivity is strongly enhanced compared to the overall loop in (e). Even more remarkable are the loop characters: while the curve in Fig. 1g resembles a normal, counterclockwise hysteresis curves, the loop in (f) is inverted [Aha94], i.e. it is cycled clockwise. Furthermore, this loop is highly asymmetric, showing a spike on the forward branch and a plateau on the backward branch. The spike is related to an intermediate backward domain wall motion within frame (A) as can be seen by following the wall motion in the image sequence (2) to (5) in Fig. 1d, while the plateau reflects wall pinning in the frame area [images (7) and (8)]. In contrast, the ribbon is magnetized by steady wall motion across the frame at location (B) [see images (6) and (9)]. The overall loops (Fig. 1a, e) may be seen as a superposition of local loops as the ones presented in (f) and (g). Note that the existence of local hysteresis loops that are cycled clockwise in some regions does not mean that these areas are energy sources inside the ribbon, because the magnetization is plotted versus the *external* applied field and not versus the local magnetic field. Therefore, the results presented in Fig. 1f do not contradict in any way the second law of thermodynamics [Ber98].

One should also notice that unusual magnetization loops have often been reported in the literature. For instance, such loops were found in amorphous Gd-Co films [Esh76], in exchange-coupled multilayers [O'S94], [Aha94], [TKF93], [WDJ01], [VAPMA01], [ZVH10], [ZLWZ04], in antiferromagnetically coupled hard/soft multilayers [KKK$^+$06]], in materials with competing anisotropies [OHH01], [NL11], [GVS98], [TKK08], and in bimodal magnetic films with a secondary grain boundary phase [MKS$^+$17]. To explain the inverted loops, several models have been proposed that are based on inhomogeneity effects [Esh76], [LHKA77], [Tog78] or on coupling effects like antiferromagnetic coupling [GO93], [TKF93], [O'S94], [PKF96], exchange coupling [TKF93], [MKS$^+$17], magnetostatic interaction [Aha94], [YX96], or anisotropy competition [NL11], [GVS98]. In some cases, it was suggested that inverted loops can also arise from experimental artifacts rather than from inhomogeneity effects [SCYP13]. However, as far as we know, *locally* inverted hysteresis loops measured by local magnetometry, have not been reported in the literature so far.

In the next section, we explore this phenomenon in a permalloy film element, which allows us again to compare the global loop with local loops but to visualize the domains of the whole sample at once.

III. Hysteresis phenomena on Permalloy film element

The MOKE hysteresis curve of a 240 nm thick Permalloy film ellipse with lateral dimensions of the order of 100 μm

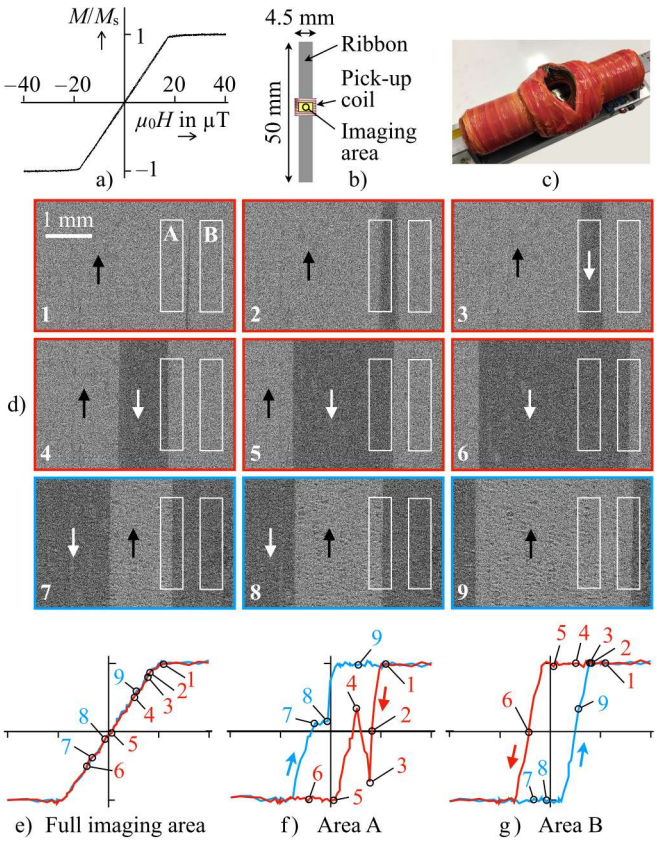

Fig. 1. Magnetometry and domains on a rapidly quenched amorphous ribbon VC6030© from Vacuumschmelze Hanau (thanks to Giselher Herzer for providing the ribbon). (**a**) Inductively measured magnetization loop at the sample location shown in (**b**) with the ribbon placed in the solenoid shown in (**c**). The images in (**d**) display selected domain states along the forward [images (1) to (6)] and backward branches [images (7) to (9)] of the MOKE loops presented in (**e, f, g**). The MOKE loops were recorded by integrating over the whole image area (e) and over local areas (f and g) with a size of 0.5×2 mm^2 as marked in (d). For the Kerr measurements, the microscope was run in the pure in-plane mode with sensitivity along the ribbon axis [SS17b]. The axis labeling of the inductive loop also applies to the MOKE loops

together with selected domain images along the loop is shown in Fig. 2. The curve was obtained by plotting the Kerr intensity of the whole element as a function of magnetic field applied along the ellipse axis, which at the same time is the axis of the Kerr sensitivity and the anisotropy axis. While reducing the magnetic field from saturation, reverse domains are nucleated at the two ends of the ellipse that are perpendicular to the field axis according to the shape anisotropy of the sample. These reverse domains grow at both ends of the ellipsis and, at around ± 1.2 mT, there are jumps in the loop that are correlated with a rapid merging of the two domains into a single inverted domain. If the magnetic field is further decreased, the element continues to be magnetized smoothly by wall motion and, approacching saturation, by rotational processes. Coercivity is very low and hardly resolved.

Similar to the case of the amorphous ribbon, the permalloy ellipse presents regular and inverted *local* hysteresis loops as show in in Fig. 3. Counterclockwise loops are observed at the left and right sides of the sample, where the magnetization

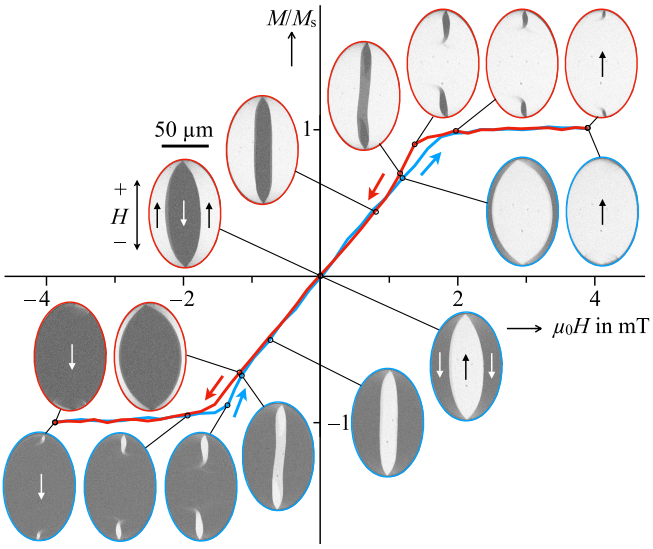

Fig. 2. MOKE hysteresis loop of a complete elliptical Permalloy film element with a thickness of 240 nm. Selected domain images along the forward and backward branches of the loop are shown. The curve was measured with a maximum field amplitude of ±20 mT to ensure saturation — plotted is just the range between ±4 mT. Like in Fig. 1, the loop and domains were recorded in the pure in-plane mode, but by using a 50x objective lens

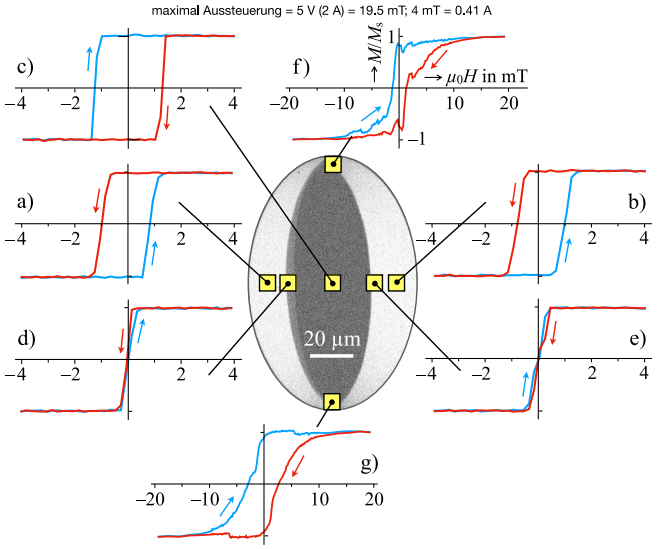

Fig. 3. Local hysteresis loops in various 7×7 μm^2 windows, obtained from the same domain images as in Fig. 2. For (f) and (g) the field axis is expanded to the maximum applied field of ±20 mT to capture also the high-coercivity loops close to the ellipse ends. The domain image shows the zero-field state

changes due to continuously moving domain walls [see curves (a) and (b) in Fig. 3]. At the center region of the ellipse, the magnetization changes by abruptly merging domains in a big Barkhausen jump and we observe an inverted loop [curve (c)]. The coercivity vanishes at specific points located in-between those locations [curves (d) and (e)]. Close to the ends of the ellipse [curves (f) and (g)], where the reversed domains are nucleated, inverted loops with high coercivity are observed. The superposition of all these clock- and counterclockwise hysteresis curves results into the total loop shown in Fig. 2.

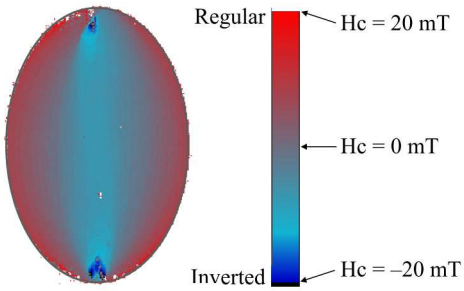

Fig. 4. Coercive field of the local hysteresis loops as a function of the location in the Permalloy element. Positive coercive fields (red) indicate counterclockwise hysteresis loops, while negative coercive fields (blue) indicate clockwise (inverted) loops

A detailed, quantitative mapping of the local loop character and coercivity is presented by a color-coded plot in Fig. 4. In this figure, the local loops were evaluated by combining the intensity of 2×2 camera pixels of the Kerr microscope, corresponding physically to 0.05 μm^2 spots. The figure shows that the overall, very low coercivity of the total loop of Fig. 2 is due to a cancellation of larger, local coercivities of regular and inverted loops as already found for the amorphous ribbon.

IV. Preisach Model

The most striking feature of the amorphous ribbon and Permalloy element, presented in the previous section, is that the superposition of highly irreversible hysteretic systems results into a reversible system.

Indeed, if we divide (or discretize) the ribbon or film into a finite set of n small regions (or finite elements), where each region represents the area of the window where the local hysteresis is measured by MOKE experiments, the total magnetic moment of the sample can be written as

$$m[h(t)] = \sum_{i=1}^{n} m_i[h(t)]\,, \qquad (1)$$

with $h(t)$ being the externally applied magnetic field and $m_i[h(t)]$ the magnetic moment of each region (element). In this equation, $m[h(t)]$ and $m_i[h(t)]$ should be regarded as functionals that act on the space of all possible applied fields $h(t)$ and not as functions of the current value of the magnetic field. In the case of the amorphous ribbon and Permalloy film, operator $m[h(t)]$ is reversible in the sense that its value depends only on the current value of the magnetic field, while the operators $m_i[h(t)]$ are irreversible and, depending on the index i, are represented by either clockwise or counterclockwise hysteresis loops.

The mentioned feature of the ribbon and film can be understood in the framework of the classical Preisach model, which expresses the total magnetic moment of a material as the superposition of a reversible set of operators described by the a function $R(\alpha)$ and an irreversible set of operators described by a two-dimensional distribution function $P(\alpha, \beta)$ according to

$$m[h(t)] = \int_{-\infty}^{\infty} R(\alpha)d\alpha + \iint_{\alpha>\beta} \hat{\gamma}_{\alpha\beta}[h(t)]P(\alpha,\beta)d\alpha d\beta\,, \qquad (2)$$

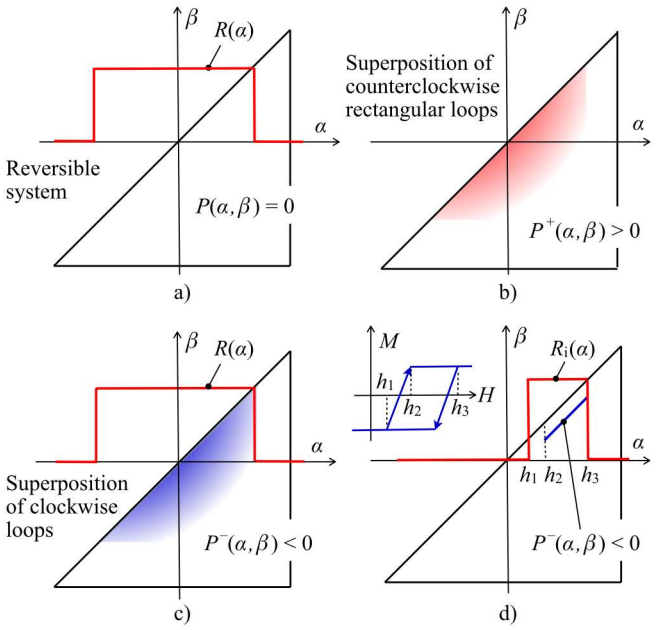

Fig. 5. Decomposition of the initial Preisach distribution of the Permalloy film element (**a**) into the two Preisach distributions shown in (**b**) and (**c**). In addition, the Preisach distribution show in (c) can be decomposed as a superposition of elementary Bouc-Wen operators, such as the one shown in (**d**)

where $\hat{\gamma}_{\alpha\beta}$ is the classical (counterclockwise) rectangular hysteresis operator defined as $\hat{\gamma}_{\alpha\beta}[h(t)] = 1$ if $h(t) > \alpha$ or $h(t) \in [\beta, \alpha]$ and $h(t_-) = \alpha$, and -1 if $h(t) < \beta$ or $h(t) \in [\beta, \alpha]$ and $h(t_-) = \beta$. In these equations, α and β are the "up" and "down" switching values of the applied field and t_- is the value of the time at the last switching point [May03]. Function $R(\alpha)$ is usually called the reversible component of the Preisach distribution, while $P(\alpha, \beta)$ is the irreversible component of the distribution. It is easy to show that, if we neglect the small irreversible processes around $h = \pm 1.6\,\mu_0 H$, the elliptical Permalloy film from Fig. 2 can be described by the Preisach model, in which the reversible component is shown by a continuous red line in Fig. 5a and the irreversible component, $P(\alpha, \beta)$, is equal to zero.

Next, we express the total magnetic moment of the film as a summation of local components $m_i[h(t)]$, in which each component is given by a "local" Preisach model, which contains both reversible and irreversible distributions. To this goal we split the Preisach distribution shown in Fig. 5a into the two Preisach distributions shown in (b) and (c), in which the first distribution represents a superposition of elementary counterclockwise hysteresis loops and the second distribution is a superposition of clockwise hysteresis loops. For this split to describe correctly the original Permalloy film we need $P^+(\alpha, \beta) + P^-(\alpha, \beta) = 0$ and, at the same time, the combined reversible and irreversible Preisach distributions shown in Fig. 5c $[R(\alpha)$ and $P^-(\alpha, \beta)]$ to model a superposition of the "elementary Bouc-Wen" operators shown in the inset of Fig. 5d. Notice that the "elementary Bouc-Wen" operators satisfy the whipping out and congruency theorems and are equivalent to a Preisach model given by the reversible $R_i(\alpha)$ and irreversible $P_i^-(\alpha, \beta)$ components shown in Fig. 5d [DA13]. With these notations we can write

$$m[h(t)] = \sum_{i=1}^{n} \iint\limits_{\alpha>\beta} \hat{\gamma}_{\alpha\beta}[h(t)] P_i^+(\alpha,\beta) d\alpha d\beta + \sum_{i=1}^{n} \left[\int\limits_{-\infty}^{\infty} R_i(\alpha) d\alpha + \iint\limits_{\alpha>\beta} \hat{\gamma}_{\alpha\beta}[h(t)] P_i^-(\alpha,\beta) d\alpha d\beta \right], \tag{3}$$

where the first sum in the right hand side represents a superposition of counterclockwise hysteresis loops, while the second sum represents a superposition of clockwise loops.

The last equation shows explicitly how the total magnetic moment of the sample is distributed throughout the magnetic ribbon and Permalloy film. Therefore, by fitting the results of local MOKE measurements with the i-th term in the last equation, we can identify the reversible and irreversible Preisach distributions at each location of the film. This fitting allows us to assign a location for each hysteron of the original Preisach distribution (which in our case contains only the reversible component) to a location inside the Permalloy film. For instance, since the MOKE measurements show that locations (f), (c) and (g) in Fig. 3 are described by clockwise hysteresis loops, it means that the hysterons of the reversible Preisach distribution $R(\alpha)$ are mostly "located" in these regions [the rest of the hysterons being located at locations (d) and (e)]. Since locations (a) and (b) are described by rectangular counterclockwise hysteresis loops, the hysterons corresponding to these regions will annihilate the negative hysterons that enter into the clockwise hysteresis model describing regions (f), (c) and (g), i.e. $\sum_{i=1}^{n}[P_i^+(\alpha,\beta) + P_i^-(\alpha,\beta)] = 0$, and do not have any correspondent on the reversible Preisach distribution.

V. Conclusion

Soft magnetic materials such as amorphous ribbons and Permalloy films have very little or zero coercive field. However, such materials can display highly nonlinear and irreversible *local* hysteresis loops. Using MOKE magnetometry in a wide-field magneto-optical Kerr microscope, we were able to measure and compare the local hysteresis loops with the global magnetic loop of a magnetostriction-free amorphous ribbon and an elliptical permalloy film element. At the same time the magnetic domains along the magnetization curves were imaged thus visualizing the processes that were responsible for the measured hysteresis loops. For both materials, local counterclockwise and clockwise hysteresis loops with a large variety of coercivities were observed. These local loops sum up to the overall, very low-coercivity total loops. Petru: please dadd some words about the Preisach model

Our investigations furthermore show that MOKE magnetometry in general has to treated with extreme care. If only local sample spots are measured, which is usually the case in a MOKE magnetometer, the obtained hysteresis curves are not representative for the whole specimen. In case of bulk materials, one has also to consider the surface sensistivity of MOKE magnetometry.

ACKNOWLEDGMENT

I.S. is grateful to DFG (German Research Foundation) for supporting this work through project SO 1623/2-1

REFERENCES

[Aha94] A. Aharoni. Exchange anisotropy in films, and the problem of inverted hysteresis loops. *J. Appl. Phys.*, 76:6977, 1994.

[Ber98] G. Bertotti. *Hysteresis in Magnetism*. Academic Press, San Diego, 1998.

[DA13] M. Dimian and P. Andrei. *Noise-Driven Phenomena in Hysteretic Systems*. Springer, New York, 2013.

[Esh76] S. Esho. Anomalous magneto-optical hysteresis loops of sputtered gd-co films. *Jpn. J. Appl. Phys*, 15:93, 1976.

[GO93] C. Gao and M.J. O'Shea. Inverted hysteresis loops in coo-based multilayers. *J. Magn. Magn. Mat.*, 127:181–189, 1993.

[GVS98] J. Geshev, A.D.C. Viegas, and J.E. Schmidt. Negative remanent magnetization of fine particles with competing cubic and uniaxial anisotropies. *J. Appl. Phys.*, 84:1488, 1998.

[HR13] Rainer Hilzinger and Werner Rodewald. *Magnetic Materials: Fundamentals, Products, Properties, Applications*. Publicis Publishing, Erlangen, 2013.

[HS98] A. Hubert and R. Schäfer. *Magnetic Domains: The Analysis of Magnetic Microstructures*. Springer, New York, 1998.

[KKK+06] D.Y. Kim, C.G. Kim, C.O. Kim, S.S. Yoon, M. Naka, M. Tsunoda, and M. Takahashi. Negative coercivity characteristics in antiferromagnetic coupled hard/soft multilayers. *J. Magn. Magn. Mat.*, 304:e356–e358, 2006.

[KSFH15] W. Kuch, R. Schäfer, P. Fischer, and F.U. Hillebrecht. *Magnetic Microscopy of Layered Structures*. Springer, Berlin Heidelberg, 2015.

[LHKA77] O. Lutes, J. Holmen, R. Kooyer, and O. Aadland. Inverted and biased loops in amorphous gd-co films. *IEEE Trans. Magn.*, 13:1615–1617, 1977.

[LSB+15] E. Lopatina, I. Soldatov, V. Budinsky, M. Marsilius, L. Schultz, G. Herzer, and R. Schäfer. Surface crystallization and magnetic properties of $fe_{84.3}cu_{0.7}si_4b_8p_3$ soft magnetic ribbons. *Acta Materialia*, 96:10–17, 2015.

[May03] I.D. Mayergoyz. *Mathematical Models of Hysteresis and Their Applications*. Elsevier Science Inc., New York, 2003.

[MKS+17] T. Maity, D. Kepaptsoglou, M. Schmidt, Q. Ramasse, and S. Roy. Observation of complete inversion of the hysteresis loop in a bimodal magnetic thin film. *Phys. Rev. B*, 95:100401, 2017.

[MSTS15] D. Marko, I. Soldatov, M. Tekielak, and R. Schäfer. Stray-field-induced faraday contributions in wide-field kerr microscopy and -magnetometry. *J. Magn. Magn. Mat.*, 396:9–15, 2015.

[NL11] Y.J. Nam and S.H. Lim. Negative remanent magnetization in a single domain particle with two uniaxial anisotropies. *Appl. Phys. Lett.*, 99:092503, 2011.

[OHH01] S. Ohkoshi, T. Hozumi, , and K. Hashimoto. Design and preparation of a bulk magnet exhibiting an inverted hysteresis loop. *Phys. Rev. B*, 64:132404, 2001.

[O'S94] M.J. O'Shea. Inverted hysteresis in magnetic systems with interface exchange. *J. Appl. Phys.*, 75:6673, 1994.

[PKF96] P. Poulopoulosa, R. Krishnan, and N.K. Flevaris. Antiferromagnetic-like coupling evidence in a pd_6ni_6 multilayer with inverted hysteresis features. *J. Magn. Magn. Mat.*, 163:27–31, 1996.

[Sch07] Rudolf Schäfer. *Investigation of Domains and Dynamics of Domain Walls by the Magneto-optical Kerr-effect*. John Wiley & Sons, Ltd, 2007.

[SCYP13] C. Song, B. Cui, H. Y. Yu, and F. Pan. Completely inverted hysteresis loops: Inhomogeneity effects or experimental artifacts. *J. Appl. Phys.*, 114:183906, 2013.

[SS17a] I. Soldatov and R. Schäfer. Advanced moke magnetometry in wide-field kerr-microscopy. *J. Appl. Phys.*, 122:153906, 2017.

[SS17b] I. Soldatov and R. Schäfer. Selective sensitivity in kerr microscopy. *Rev. Scient. Instr.*, 88:073701, 2017.

[TKF93] K. Takanashi, H. Kurokawa, and H. Fujimori. A novel hysteresis loop and indirect exchange coupling in co/pt/gd/pt multilayer films. *Appl. Phys. Lett.*, 63:1585, 1993.

[TKK08] L.V. Tho, C.G. Kim, and C.O. Kim. Investigation of negative coercivity in one layer formation of soft and hard magnetic materials. *J. Appl. Phys.*, 103:07B906, 2008.

[Tog78] Y. Togami. Stability of small bits written in amorphous gdco thin films. *Appl. Phys. Lett.*, 32:673, 1978.

[VAPMA01] S.M. Valvidares, L.M. A?lvarez-Prado, J.I. Martn, and J.M. Alameda. Inverted hysteresis loops in magnetically coupled bilayers with uniaxial competing anisotropies: Theory and experiments. *Phys. Rev. B*, 64:134423, 2001.

[WDJ01] Y.Z. Wu, G.S. Dong, and X.F. Jin. Negative magnetic remanence in co/mn/co grown on gaas(001). *Phys. Rev. B*, 64:214406, 2001.

[YX96] X. Yan and Y. Xu. Negative remanence in magnetic nanostructures. *J. Appl. Phys.*, 79:6013, 1996.

[ZLWZ04] R.K. Zheng, H. Liu, Y. Wang, and X.X. Zhang. Inverted hysteresis in exchange biased coated cr_2o_3 coated cro_2 particles. *J. Appl. Phys.*, 96:5370, 2004.

[ZVH10] M. Ziese1, I. Vrejoiu, and D. Hesse. Inverted hysteresis and giant exchange bias in $la_{0.7}sr_{0.3}mno_3$/$srruo_3$ superlattices. *Appl. Phys. Lett.*, 97:052504, 2010.